Review Article

Hiroo Kinoshita*, Takeo Watanabe and Tetsuo Harada

Development of element technologies for EUVL

DOI 10.1515/aot-2015-0027
Received March 24, 2015; accepted May 13, 2015; previously published online July 1, 2015

Abstract: Thirty years have passed since the first report on extreme ultraviolet lithography (EUVL) was presented at the annual meeting of the Japanese Society of Applied Physics in 1986. This technology is now in the manufacturing development stage. The high-volume manufacturing of dynamic-random-access-memory (DRAM) chips with a line width of 15 nm is expected in 2016. However, there are critical development issues that remain: generating a stand-alone EUV source with a higher power and producing a mask inspection tool for obtaining zero-defect masks. The Center for EUVL at the University of Hyogo was established in 2010. At present, it utilizes various types of equipment, such as an EUV mask defect inspection tool, an interference-lithography system, a device for measuring the thickness of carbon contamination film deposited by resist outgassing, and reflectivity measurement systems.

Keywords: defect; EUVL; exposure system; interference lithography; mask; phase defect; reflectivity; resist.

1 Introduction

Thirty years have passed since the first report on extreme ultraviolet lithography was presented at the annual meeting of the Japanese Society of Applied Physics in 1986 [1]. In the early stages, Kinoshita and his colleagues at the Nippon Telegraph and Telephone Corporation worked on developing basic component technologies, such as aspherical-mirror optics, Mo/Si multilayer coatings, reflective masks, and chemically amplified resists [2–6]. In 1995, an optical system with two aspherical mirrors was used to replicate 0.1-μm patterns in a large 10-mm^2 exposure area [7, 8].

The Himeji Institute of Technology, in collaboration with Nikon and the Hitachi Central Laboratory, developed an experimental exposure tool with three aspherical mirrors at the NewSUBARU synchrotron facility. In 2000, the ASET EUVL project, launched in 1998, used this exposure tool to fabricate 40-nm isolated lines. Then, in 2001 the Extreme Ultraviolet Limited Liability Company (EUV-LLC) succeeded in replicating 39-nm isolated lines. Polishing and measurement technologies for aspherical mirrors have improved to dimensions as small as 0.1 nm, and the technology for multilayer films has yielded a reflectance near the theoretical value, owing to the progress in thin film technology for semiconductors in the 1990s.

Based on these achievements, the full-scale development of an exposure tool began in 2002. Currently, this technology is in the manufacturing development stage. ASML has already delivered six beta-level EUVL scanners to semiconductor manufacturing companies, and the fabrication of DRAMs has begun. Although the light source and a mask inspection tool for zero-defect masks require further development, the movement toward the mass production of devices has begun.

Work on resists and a mask-defect inspection tool began in 2002. Many years later, the Center for EUVL at the University of Hyogo was established in 2010. Since then, the Center has carried out exposure and evaluation experiments related to EUVL on the BL-3, -9, and -10 beamlines of the NewSUBARU.

BL-3 uses a bending magnet to make a light source. It is equipped with EUV microscopy (EUVM) and EUV coherent scatterometry microscopy (CSM) systems. The EUVM system was first developed to inspect the absorber pattern of finished EUV masks and to detect phase defects in multilayer blanks. The resolution for pattern defects is 60 nm, and it can detect pit-type phase defects with a width of 40 nm and height of 1 nm. The CSM system employs a high-order harmonic generation (HHG) 13.5-nm coherent source to detect pattern defects and measure the critical dimension of patterns.

***Corresponding author: Hiroo Kinoshita,** Center for Extreme Ultraviolet Lithography, University of Hyogo, Ako-gun, Hyogo, Japan, e-mail: kinosita@lasti.u-hyogo.ac.jp
Takeo Watanabe and Tetsuo Harada: Center for Extreme Ultraviolet Lithography, University of Hyogo, Ako-gun, Hyogo, Japan

www.degruyter.com/aot
© 2015 THOSS Media and De Gruyter

BL-9 uses a 10.8-m long undulator to make a light source. Given that this beamline has a high spatial coherence, an EUV interference lithography (EUV-IL) system is installed here. A system for measuring the thickness of carbon contamination film deposited by outgassing from a resist irradiated with a strong light source equivalent to that of a lithography tool for mass production was also developed on this beamline in collaboration with EIDEC.

BL-10 uses a bending magnet to make a light source. The three grating monochromators (600, 1800, and 2400 lines/mm) at the front end of the beamline enable very accurate measurements of the reflectivity of optical elements, such as multilayer masks. The reflectivity characteristics are calibrated with a standard CXRO sample. Moreover, in collaboration with EIDEC, a study has been launched on the use of a focused coherent beam for the three-dimensional imaging of phase defects in EUVL mask blanks.

This article reviews recent work on EUVL at the NewSUBARU.

2 Three-aspherical-mirror system

The Himeji Institute of Technology, in collaboration with Hitachi Central Laboratory and Nikon, developed a three-aspherical mirror system [9–13] called the ETS-1 (Figure 1). It consists of illumination optics, mask and wafer scanning stages, mask and wafer alignment optics, a reduction camera, and a load-lock chamber for loading wafers. The reduction camera contains three aspherical mirrors. The magnification of the optics is 1/5. There is a distortion-free area with a resolution of <0.01 µm in a ring image field that is 1.0 mm wide and 30 mm long on a wafer. By moving the mask stage in synchronization with the wafer stage, an exposure area of 30 mm×38 mm can be illuminated.

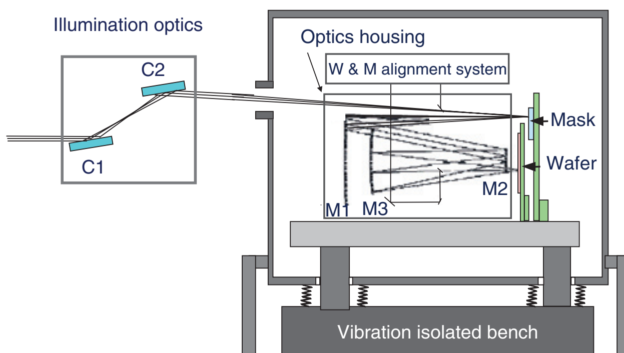

Figure 1: Configuration of the large exposure system of EUVL.

The mask stage has five degrees of freedom. The Y-axis is used for scanning the mask, and the Z-axis is for focusing and magnification alignment. The wafer stage consists of course- and fine positioning stages. The coarse-positioning stage is driven by a pulse motor and has a mechanical bearing guide; while the Z-axis has a measurement system with a resolution of 0.1 µm. The fine-positioning stage for mask and wafer alignment and focus alignment employs a piezoelectric transducer, which provides a resolution of 1 nm in the X- and Y-directions and 10 nm in the Z-direction. The photograph in Figure 2 shows an overview of the system. The system is in a thermal clean chamber with a temperature variation of ±0.1°C. The dimensions of the chamber are approximately 1 m×1.2 m×1 m.

ASET, which was a consortium of semiconductor companies supported by NEDO, used the ETS-1 to investigate the characteristics of EUVL masks and resists. In 2000, The Himeji Group and ASET succeeded in replicating 60-nm line-and-space (L/S) patterns (Figure 3) and 40-nm isolated lines (Figure 4) in a large 10-mm^2 area. In 2001, EUV-LLC managed to replicate 39-nm isolated lines. Moreover, three large scanner companies have begun developing a practical system.

3 Development of EUV resist and EUV-IL

Intensive work on EUV resists was carried out to increase the performance to a level suitable for high-volume production [14–20]. These resists exhibit a trade-off among resolution, linewidth roughness, and sensitivity.

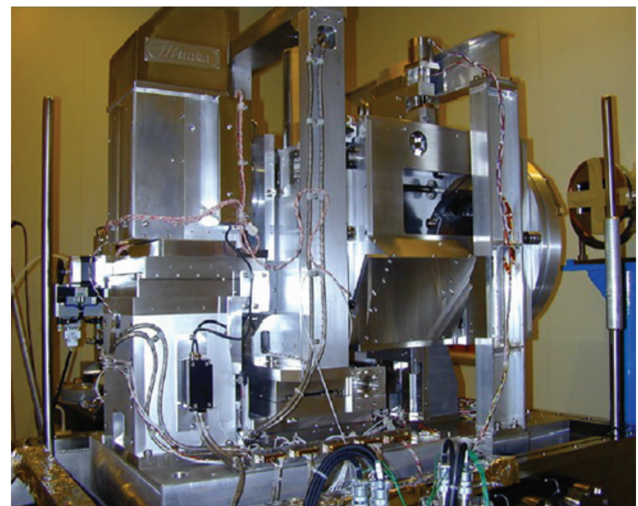

Figure 2: Overview of large exposure system of EUVL.

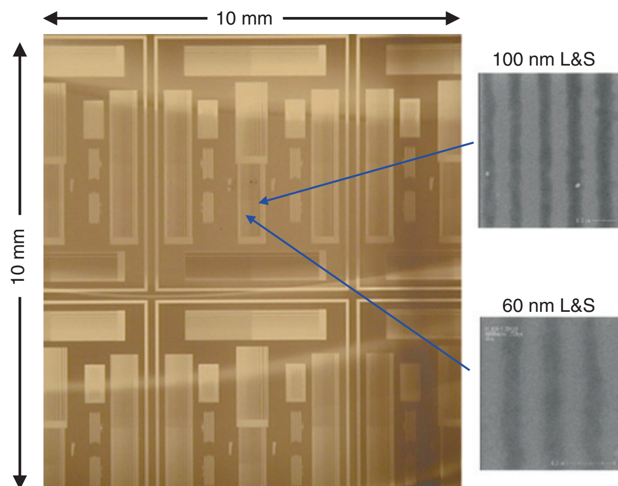

Figure 3: Replicated pattern of large exposure area.

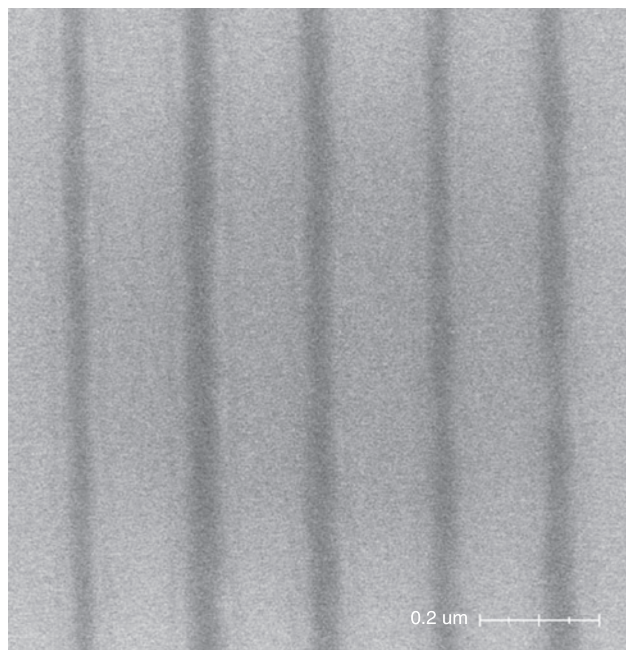

Figure 4: Replicated pattern of 40-nm isolated line.

The ETS-1 exposure system at the NewSUBARU, developed in 1998, was used to test various resists. In collaboration with the ASET EUVL Group, it was found that a chemically amplified (CA) resist was suitable for EUVL. First, the replication of 40-nm isolated lines was demonstrated using the ETS-1. Then, work was begun on the development of a new resist with a high sensitivity, a small linewidth roughness, and low outgassing.

The key to reducing the line edge roughness (LER) of a CA resist is the uniformity of the photoreaction during EUV exposure. In a CA resist, the photochemical reaction is initiated by a photo-acid generator (PAG). Thus, the density of the PAG inside the resist film must be uniform to obtain a low LER.

The world's first PAG-bound polymer resist for the EUV region, based on the polyhydroxystyrene system, was reported in 2006. This PAG-bound polymer resist exhibits a lower LER and a higher sensitivity than a PAG-blended polymer resist for EB exposure (Figure 5) [17–20]. In the former, the cation of the PAG is bonded indirectly to the base polymer via a functional group. A 50-keV electron direct-writing tool (Figure 6) was used to replicate a 22.5-nm L/S pattern; an LER of 3.6 nm, and a sensitivity of 32 $\mu C/cm^2$ were obtained. This PAG-bound polymer is now commonly used in EUVL because it provides a low LER.

To evaluate resist performance for the hp 22-, 16-, and 11-nm nodes, an EUV interference lithography (EUV-IL) system was developed on BL-9 (Figure 7) [21–24]. The undulator light is 1000 times more intense than that produced by a bending magnet, and it has a very high spatial coherence. A Young's interference experiment revealed the spatial coherence length to be >1 mm. The system employs two window-type transmission gratings fabricated at the Center for EUVL.

In the design of an interference exposure system employing a transmission grating, the effect of Fresnel diffraction from the opening must be taken into account. This is because a Fresnel diffraction pattern is generated

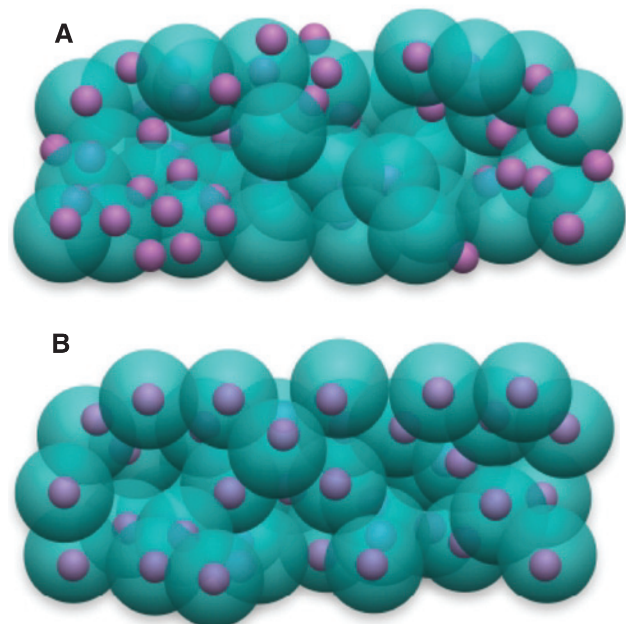

Figure 5: (A) PAG-blended resist, (B) PAG-bound resist.

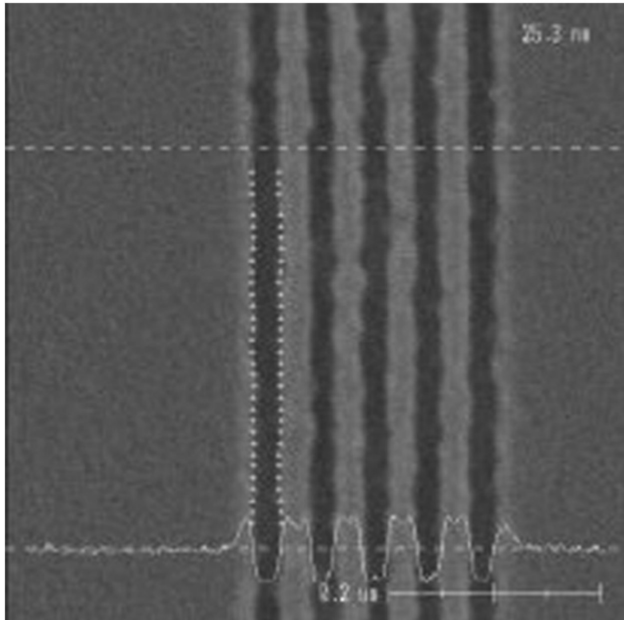

Figure 6: Exposure pattern of PAG-bound resist: 22.5-nm L/S.

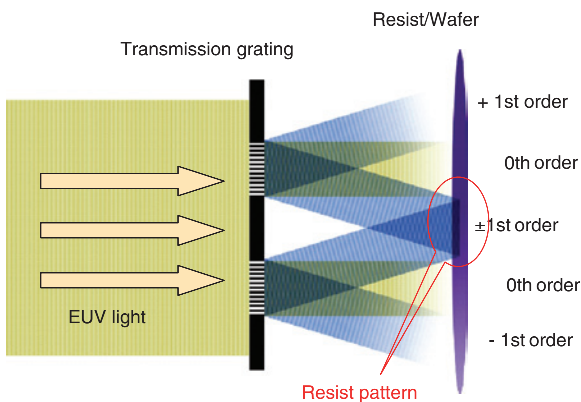

Figure 7: Principle of EUV interference lithography.

when the opening is very close to the surface of a wafer. The effects of Fresnel diffraction can be calculated using the following equations:

$$\mathrm{I}(x,y)=\frac{I_0}{4}\{|C(u_2)-C(u_1)|^2+|S(u_2)-S(u_1)|^2\}$$
$$\times\{|C(v_2)-C(v_1)|^2+|S(v_2)-S(v_1)|^2\}$$

$$\mathrm{C}(w)\equiv\int_0^w \cos(\pi w'^2/2)dw'$$

$$\mathrm{S}(w)\equiv\int_0^w \sin(\pi w'^2/2)dw'$$

$$u_1=-\sqrt{2}\times\left(\sqrt{N_x}+\frac{x}{\sqrt{\lambda D}}\right)$$

$$u_2=\sqrt{2}\times\left(\sqrt{N_x}-\frac{x}{\sqrt{\lambda D}}\right)$$

$$v_1=-\sqrt{2}\times\left(\sqrt{N_y}+\frac{y}{\sqrt{\lambda D}}\right)$$

$$v_2=\sqrt{2}\times\left(\sqrt{N_y}-\frac{y}{\sqrt{\lambda D}}\right)$$

$$N_x=\frac{m}{4\lambda D}$$

$$N_y=\frac{n}{4\lambda D}$$

$$\mathrm{Contrast}=\frac{I_{\max}-I_{\min}}{I_{\max}+I_{\min}}=\frac{2I_2}{I_1+2I_2}$$

Here, m is the length of the side of the opening, n is the width of the opening, and D is the distance between the transmission grating and the wafer.

The effect of Fresnel diffraction was calculated as a function of m (Figure 8), assuming an n of 30 µm and a D of 1 mm. The results show that, when m is 200 µm, the intensity distribution of the Fresnel diffraction does not influence the contrast of the interference fringe.

A transmission grating with a pitch as small as 30 nm was also fabricated. Two resist patterns were replicated for the hp 15-nm node using (a) a negative resist from Inpria, and (b) a positive resist from Idemitsu Oil & Gas (Figure 9).

4 Actinic mask inspection system using Schwarzschild optics

An EUVL mask is fundamentally different from masks for KrF, ArF, and other kinds of DUV lithography because it is a reflective type. It is composed of an absorber layer on top and a reflective multilayer film formed on a 6025 glass substrate. If pits or bump defects appear during the glass fabrication process, or if there are foreign particles present during the deposition process, they become phase defects after the deposition of the multilayer film. Phase defects cannot be detected using a DUV inspection tool because DUV light does not penetrate far enough into the multilayer.

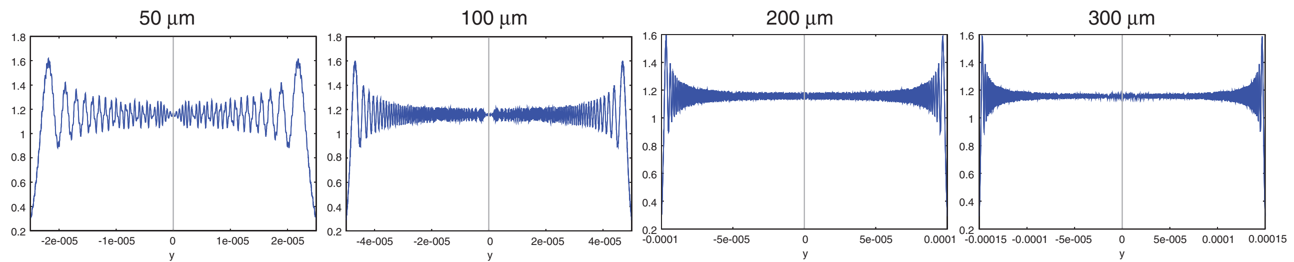

Figure 8: Fresnel effect on interference lithography.

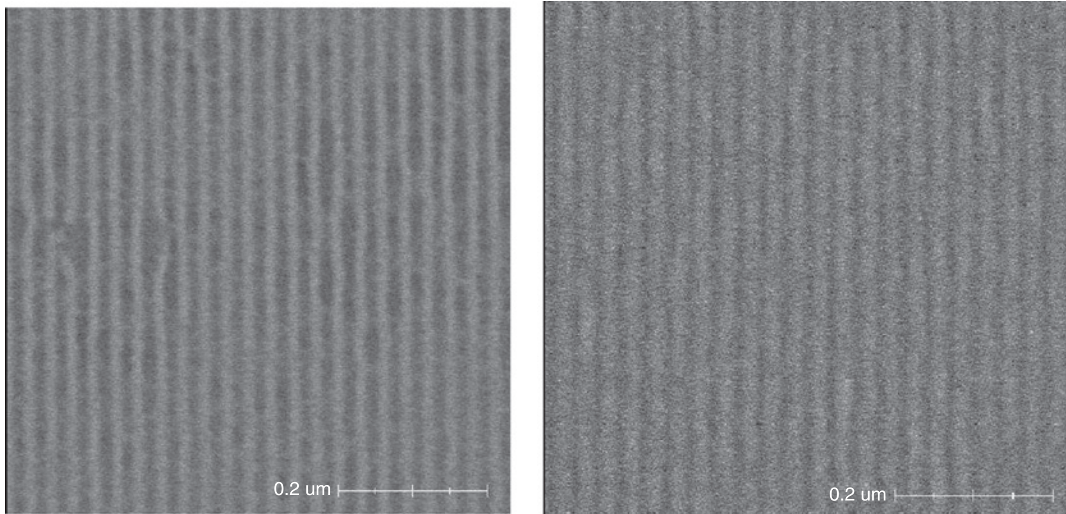

Figure 9: Exposure results obtained with EUV-IL.
(A) Negative resist (Inpria), (B) Positive resist (Idemitsu).

Furthermore, there are problems specific to EUV masks. One is that, assuming an incident angle of 6° on the mask, if the direction of illumination is perpendicular to the lines on the mask, a shadowing effect occurs due to the thickness of the absorber pattern. This makes the exposed pattern slightly wider than the absorber pattern. However, if the incident light is parallel to the lines, no such effect occurs. In view of the shadowing effect, the issues concerning the inspection of EUVL masks include amplitude and phase defects.

The development of an actinic mask inspection system based on Schwarzschild optics began in 2001 [21–23] (Figure 10). The system is installed on the BL-3 beam line of the NewSUBARU and consists of Schwarzschild optics, a Mirau interferometer, an X-Y sample stage, a focus detector, an X-ray zooming tube connected to a CCD camera, and an image processing computer. It is installed in a vacuum chamber that is mounted on a vibration isolation table. The chamber is evacuated down to a pressure of 10^{-5} Pa. This system was used to determine the critical dimension of phase defects that influence

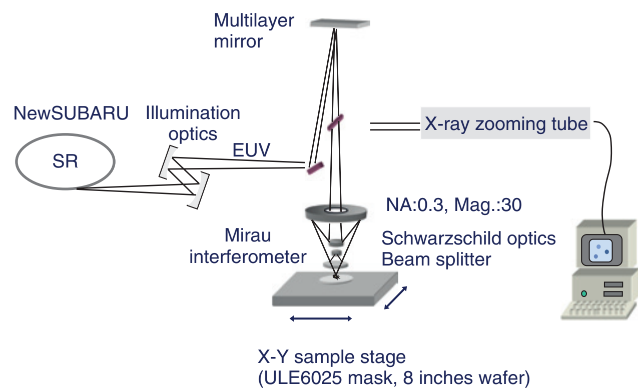

Figure 10: Configuration of the EUV microscope for actinic mask inspection.

the absorber pattern. A previous study employed a pit defect 70 nm wide and 1 nm deep (Figure 11). In collaboration with HOYA, the influence of phase defects on the absorber pattern was also investigated, and it was found that a phase defect under the absorber pattern did not influence the pattern but that a phase defect either at the

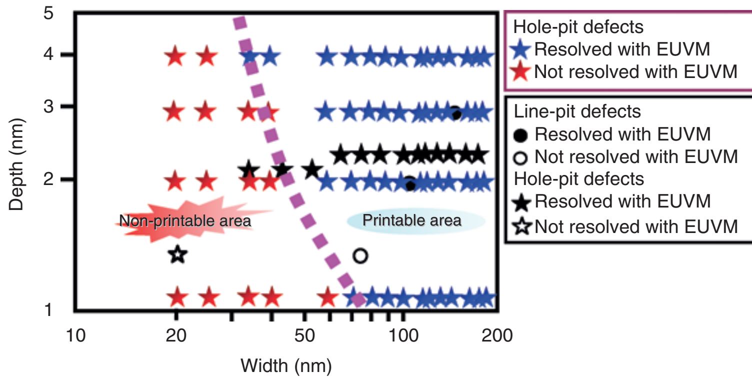

Figure 11: Critical dimension of the phase defect.

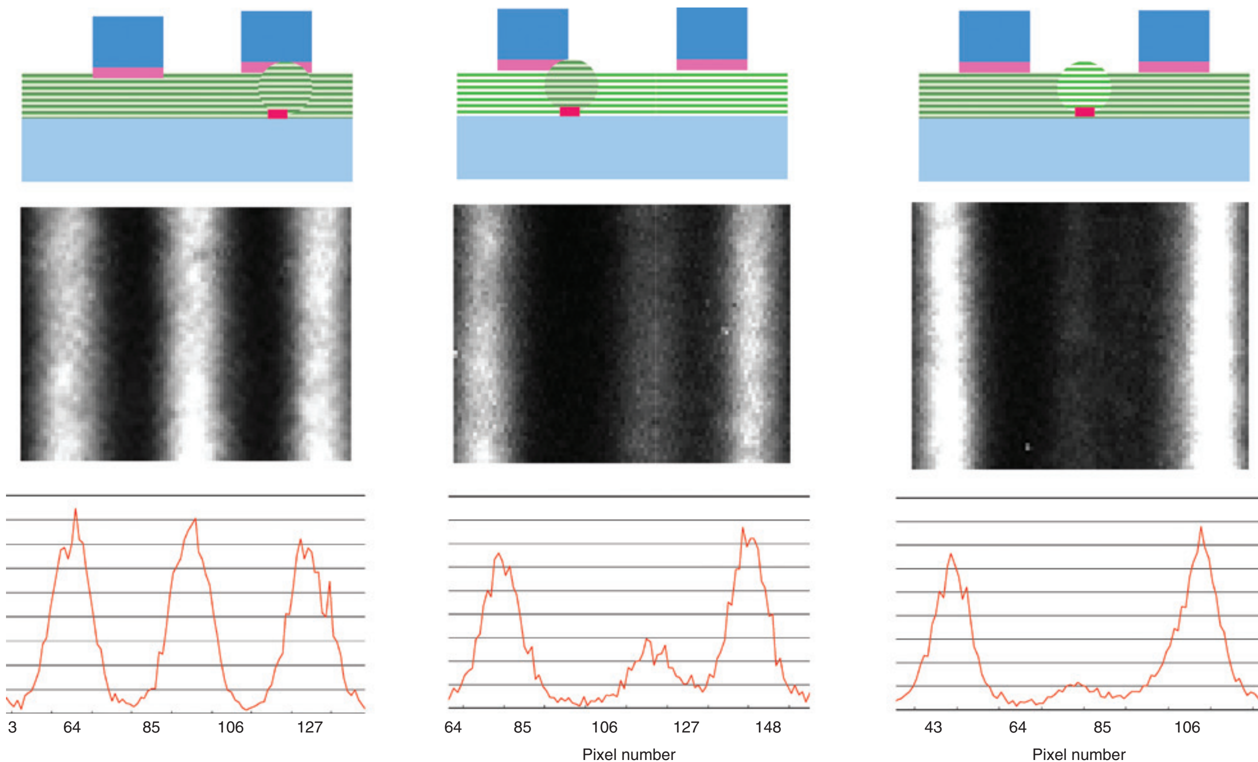

Figure 12: Effect of the phase defect on the absorber pattern.

shoulder of a pattern or between two patterns created size and bridge defects (Figure 12). Recently, these results were used to eliminate a phase defect and correct an absorber pattern.

5 Coherent scatterometry microscope

After developing a mask inspection system using reflective optics, the development focus shifted to a new-concept mask inspection system based on a coherent source and a CCD camera. This system, called a coherent scatterometry microscope (CSM), consists of a coherent EUV light source, an X-ray CCD camera, and a computer system [24–29] (Figure 13). The procedure for inspecting an EUV mask has three steps:

1. Irradiate the mask with coherent light;
2. Record the intensity distribution of the diffracted light with the CCD camera; and
3. Reconstruct an image of the absorber pattern using a computer algorithm.

This is a lensless system representing an ideal form of X-ray phase-contrast imaging because there is no

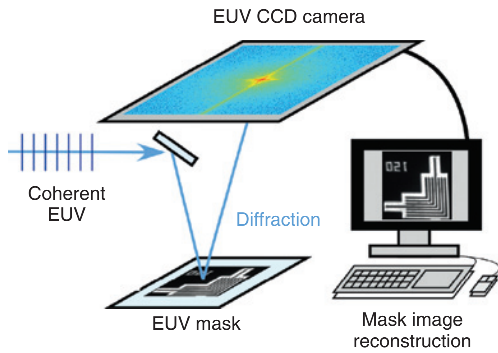

Figure 13: Principle of EUV coherent scatterometry.

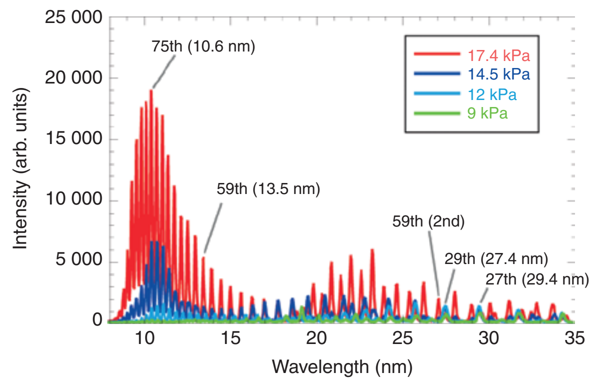

Figure 15: Characteristics of the HHG EUV light.

degradation in contrast due to lenses. Furthermore, given that high-harmonic generation (HHG) produces EUV light, the system can be set up in most laboratories.

The stand-alone HHG-CSM (Figure 14) consists of a Ti:sapphire pump laser, an HHG module for the EUV source, and a CSM. The pump laser is a commercially available Spitfire Pro (repetition frequency: 1 kHz; output power: 6 W; wavelength: 800 nm; pulse width: 32 fs, Spectra Physics Co. Ltd, Santa Clara, CA, USA). The HHG module consists of a focusing chamber, a gas cell, an EUV branch chamber, and an EUV spectrometer. The focusing chamber is the most important part. To achieve phase matching, the aperture and the curvature of the focusing mirror have to be optimized. HHG light is generated through the interaction between an fs laser pulse and the gas in the gas cell. The spectral intensity distribution and divergence are determined by the pressure of the gas. The HHG light from the chamber is filtered with a Zr thin film and a Mo/Si multilayer to yield EUV light.

Here, the intensity of the HHG EUV light was measured as a function of wavelength (Figure 15) at various pressures with He in the gas cell. He was selected on the basis of efficiency and the power of the spectral intensity distribution. For wavelengths around 10 nm, a He pressure of 17.4 kPa provides the highest intensity among the pressures tested. In HHG, the spectral intensity is high for odd harmonics, and the 59th harmonic of the Ti:sapphire laser has a wavelength of ~13.5 nm.

For fully coherent EUV light with a wavelength of 13.5 nm, the highest power obtained so far is 1 μW. This is 1000 times greater than the power of the synchrotron radiation source in the NewSUBARU. The divergence of the light is 0.17 mrad, which, to our knowledge, is the smallest value ever reported.

An image created by irradiation with coherent light is basically reconstructed by an iterative phasing method. The coherent diffraction pattern is speckled when the sample is disordered. However, a speckled

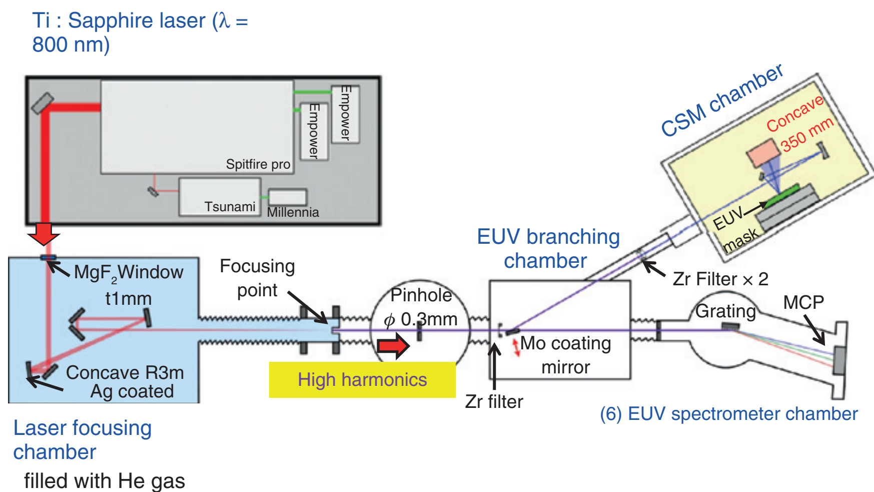

Figure 14: Configuration of the HHG-coherent scatterometry microscope.

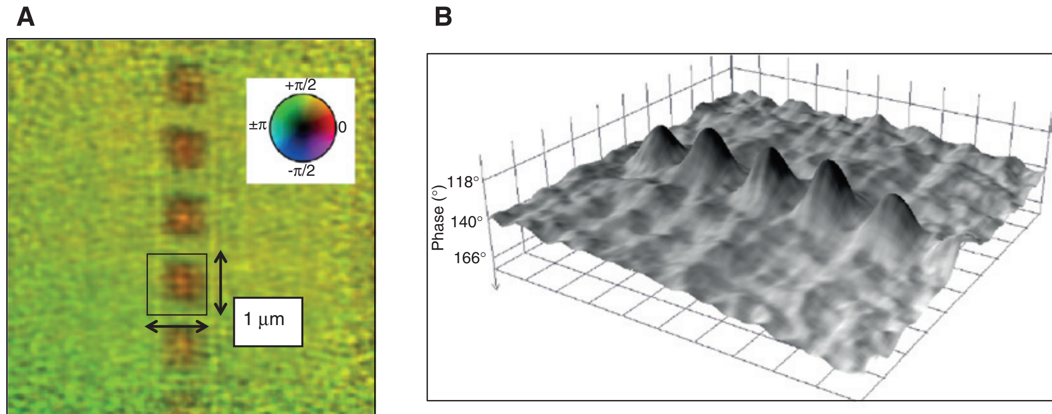

Figure 16: (A) 2D reconstruction image of phase defect, (B) 3D reconstruction image using phase information.

diffraction pattern can be sampled finely enough to satisfy the retrieval conditions. That is, the diffracted light captured by the CCD camera is only an amplitude signal. To reconstruct an aerial image of real space, the phase information must be retrieved from frequency space. Then, the inverse Fourier and Fourier transforms between frequency space and real space are iteratively calculated [14–20]. The iteration process starts from a random phase in an outer region of the irradiated area, and the area in the outer space is revised iteratively using intermediate reconstructed images. The area outside the irradiated area is set to zero as a constraint. Increasing the number of iterations improves the reconstructed image.

A coherent scatterometry microscope based on X-ray diffraction theory can produce phase information, which in turn, enables the reconstruction of a three-dimensional (3D) image of real space. Of particular note is that the phase in real space is also retrieved separately.

Figure 16 shows a reconstructed image of phase defects. The phase distribution of a 1-μm^2 defect was also reconstructed, from which the phase was quantitatively estimated. The height of these phase defects was estimated to be 6.1 nm. This value agrees well with the 6.2 nm obtained by AFM measurements.

With the previously developed inspection tool that uses SR, the width of a periodic absorber pattern can be estimated from the intensity of the light diffracted by the pattern; and it can be measured as the width of the focal pattern on a wafer. The CD of a 22-nm node L/S pattern was measured with the CSM, and the results were compared to those obtained with a CD-SEM (Figure 17). The agreement is good. Furthermore, an excellent repeatability of 0.32 nm (3σ) for the CD measurement of L/S patterns is obtained. This value satisfies the ITRS requirement of a repeatability of <0.65 nm (3σ) [26]. However, owing to the

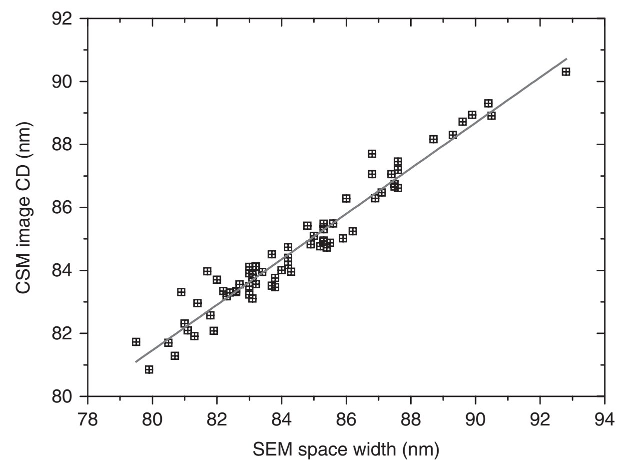

Figure 17: Correlation of CD measurements of CSM and CD-SEM.

low coherent flux of SR light, such defects as bridges and missing holes cannot be observed.

The HHG-CSM was used to inspect a downsizing defect (Figure 18). The centerline of the L/S mask pattern (Figure 18A) is 2 nm narrower than the other lines. In the corresponding diffraction pattern (Figure 18B), 0th-, +1st-, and -1st-order diffracted light appear clearly in areas where there are no defects. Furthermore, the signal from the defect is observed across the 0th- and 1st-order diffraction patterns. In the enlargement of the unclear diffraction signal surrounded by the dashed white line (Figure 18C), the red line indicates the signal for the defect, and the blue line indicates the signal for no defect. These results demonstrate that the HHG-CSM system can detect a downsizing defect as small as 2 nm.

Defect inspection commonly involves a die-to-die comparison of a number of chips. In the array of holes

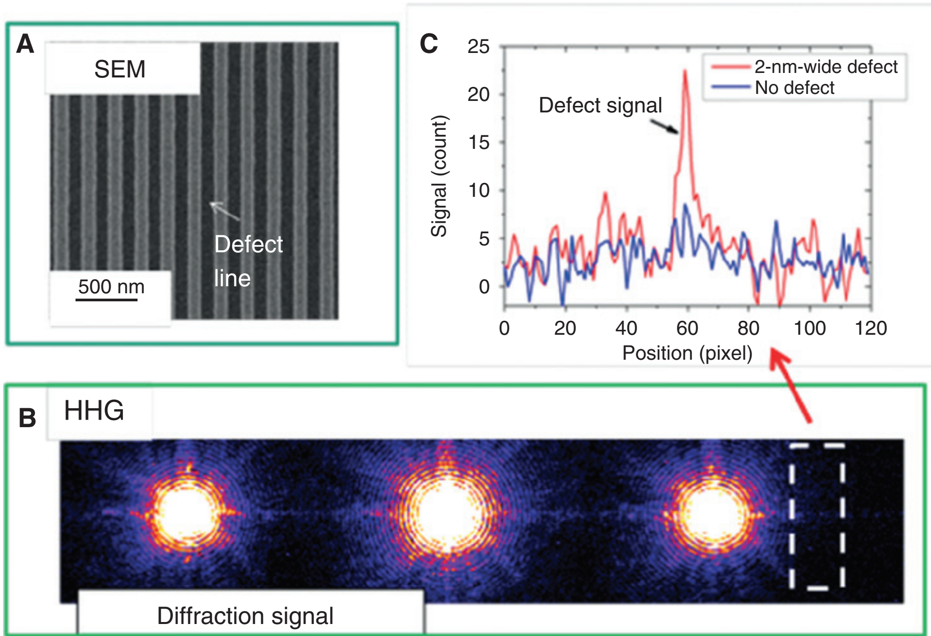

Figure 18: CSM results for 2-nm downsizing line defect.
(A) SEM image of the 22 nm node, (B) Diffraction image with downsizing defect (C) intensity distribution of diffracted light.

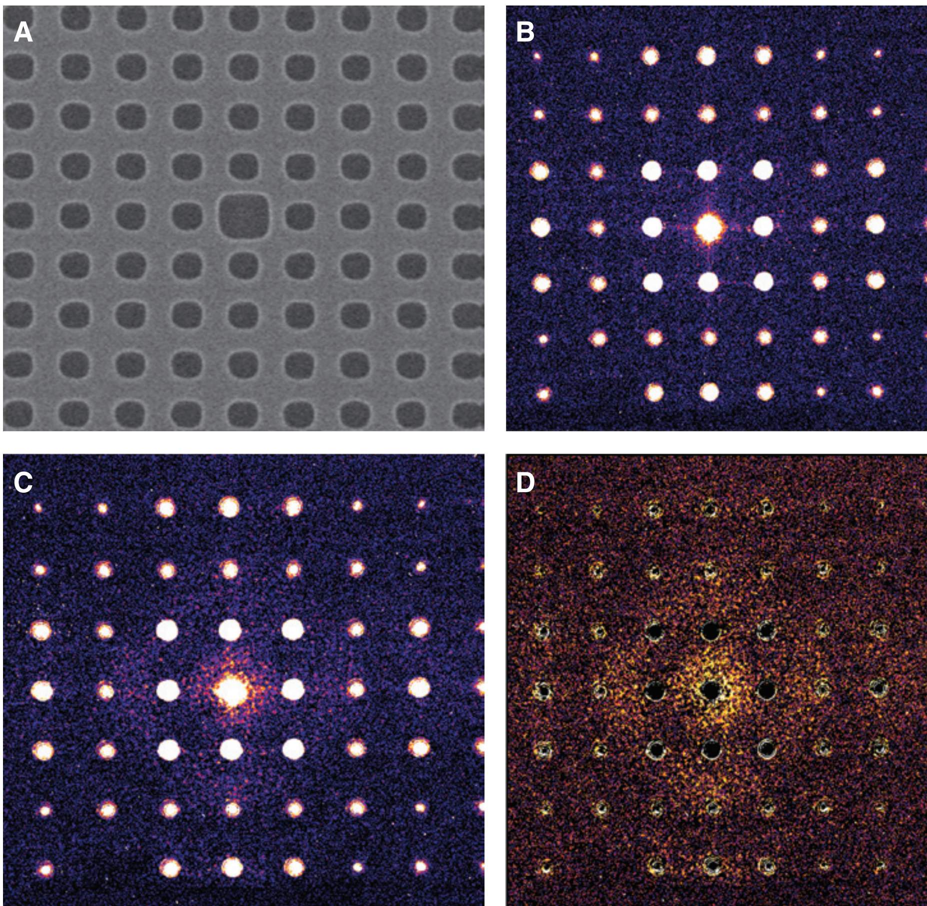

Figure 19: Results of the hole defect inspection.

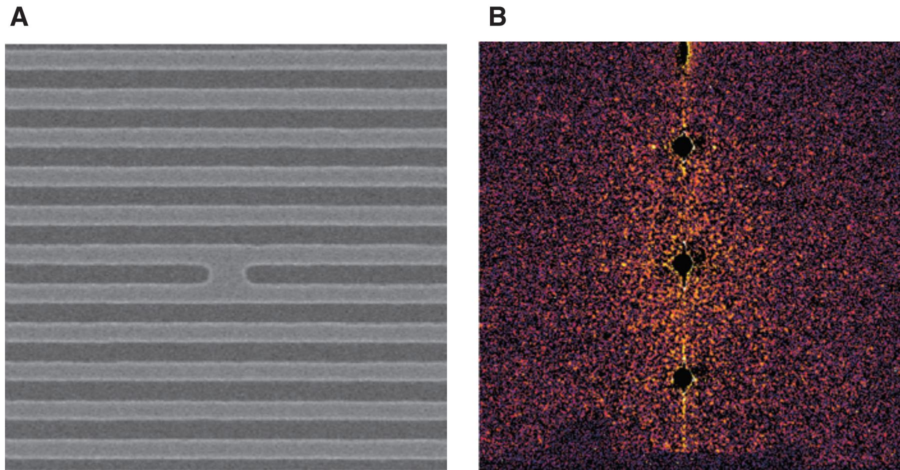

Figure 20: Results of the bridge defect inspection.

with a diameter of 88 nm in Figure 19A, the center hole is 30 nm larger than the others. A diffraction pattern was taken of a mask pattern without (Figure 19B) and of one with (Figure 19C) a defect. The former is uniform and exhibits no abnormalities. A can be seemn, the difference pattern between the two (Figure 19D) shows abnormalities resulting from the defects around the 0th and 1st orders.

For an 88-nm L/S pattern with a 130-nm-wide bridge defect (Figure 20A), differences between the diffraction patterns of samples with and without defects (Figure 20B) appear around the 0th, +1st, -1st orders. Figure 21 shows the defect resolution for various types of defects. For line-end oversize defects, defects with a size of 24 nm are observed.

As mentioned above, this system detects the diffraction signals from both periodic structures (L/S and hole patterns) and aperiodic structures, before reconstructing the images.

6 Micro-CSM

The CSM system complements an actinic mask inspection tool as a characterization tool. However, the spot size of the illumination is about 5 µm, which is too large to detect a phase defect <50 nm wide and 1 nm high, because the defect signal is much weaker than the background. This led to the development of a micro-coherent EUV scatterometry microscope (Micro-CSM) system [30], which has a focused illumination probe with a size of several hundred nanometers. This system will be used to examine the phase distribution of small defects (width: <50 nm; height: <1 nm). A schematic view of the system (Figure 22) shows that the coherent EUV illumination is focused on a mask by a Fresnel zone plate (FZP). Diffraction from a defect is recorded directly by a CCD camera. The focusing layout of the FZP is off-axis so that the reflection signal

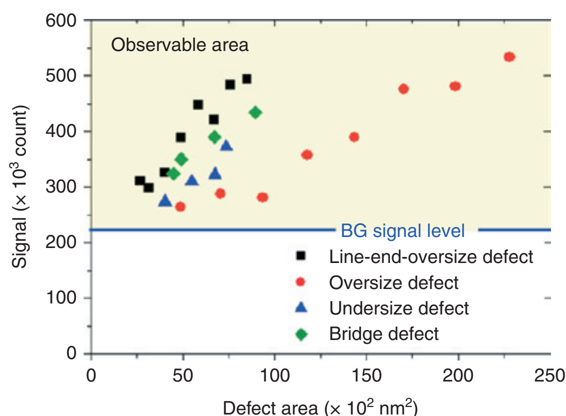

Figure 21: Detect sensitivity of various defects by CSM.

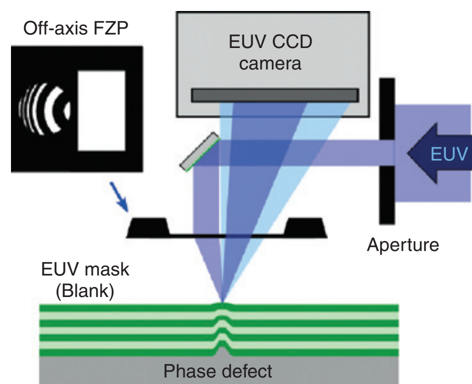

Figure 22: Configuration of the focused coherent EUV scatterometry microscope.

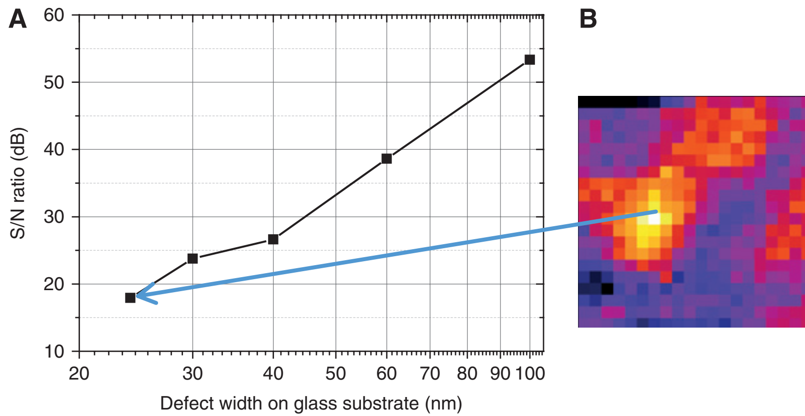

Figure 23: Detection of the sensitivity of phase defect.

can be used, and there is a window that allows reflected EUV light to enter.

The S/N ratio and noise for various sizes of programmed phase defects on the surface of a multilayer surface were measured as a function of the width of a defect on a glass substrate as measured by AFM (Figure 23A). Noise, in this case, refers to the standard deviation estimated from signal fluctuations for a region with no defects. The detection limit for a phase defect was found to be a width of 25 nm and a height of 1.4 nm. The mapping for the smallest detectable defect is shown in Figure 23B. Ptychography on this diffraction signal was used to reconstruct the phase defect. Meanwhile, Figure 24 shows the reconstructed image of a pit defect on a glass substrate. A programmed defect 100-nm wide and 3-nm high was reconstructed, and the size estimated from the reconstructed image was a width of 100 nm and a height of 5.0 nm.

7 Reflectivity measurement

As mentioned in Section 1, it is possible to estimate the reflectance of a multilayer, the transmittances of a resist and a thin film, the optical constants of a material, and the roughness of an EUV mask substrate on the BL-10 beam line of the NewSUBARU. The reflectance of a multilayer film can be obtained by cross-checking with CXRO.

The reflectance of a multilayer of La/B_4C was measured with 6.7-nm EUVL (Figure 25) [31]. The multilayer film was fabricated by Rigaku (USA). A peak reflectance close to 50% was obtained for incidence angles in the range 5°–8°at a wavelength of 6.7 nm.

Furthermore, a new reflectometer has been developed that can evaluate the condenser optics of an LPP source, which are 800 mm in diameter and 150 mm in height, and weigh 50 kg. Figure 26 shows a photograph of the largest reflectometer in the world. It was able to measure

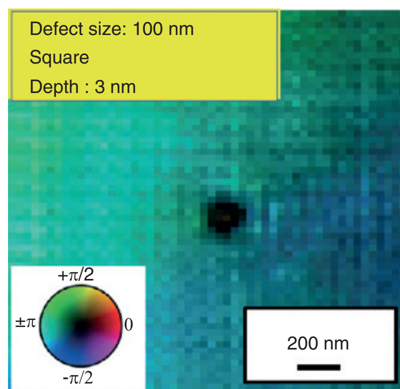

Figure 24: Reconstruction image of the phase defect.

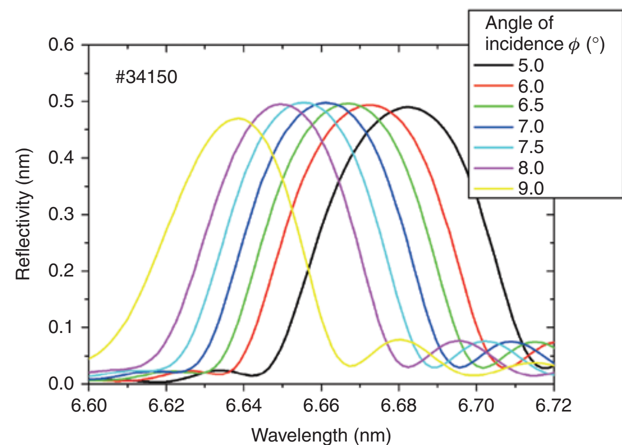

Figure 25: Reflectivity measurement of La/B4C.

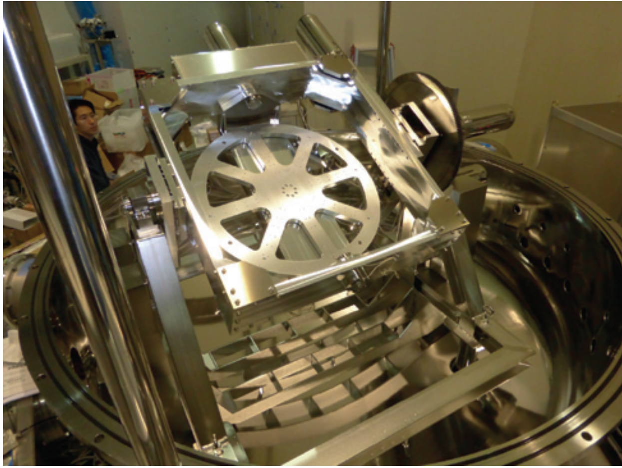

Figure 26: Photograph of a large reflectometer.

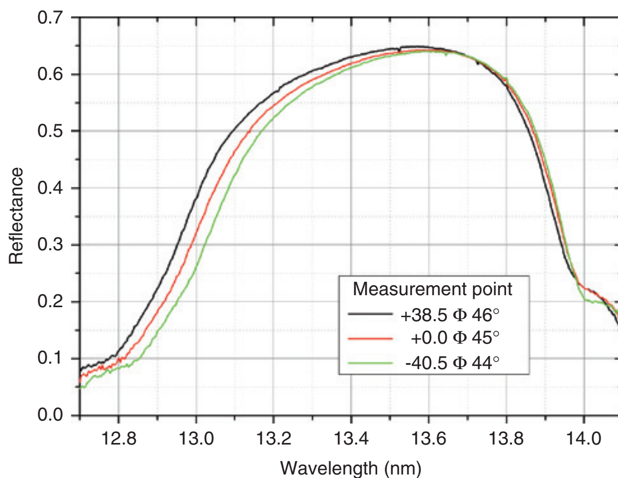

Figure 27: Reflectivity measurement of a parabolic mirror using a large reflectometer.

the reflectance of the parabolic mirror in Figure 27. The reflectivity agrees well with the value obtained by CXRO.

8 Conclusions

In conclusion, EUVL research and development over the past 30 years has led to a number of significant breakthroughs. The drive to develop a practical EUVL technology spread to both hemispheres in the latter half of the 1980s. We can now look back at the history of the early development work with a wonderful feeling of accomplishment. Although the development of the source has lagged, the outlook for the mass production of the 15-nm generation in 2016 is promising. The development of EUVL technology involves progress in and the integration of nanotechnologies; thus, spillover from the semiconductor industry to environmental technology, energy, and biotechnology is anticipated. The authors hope to continue pursuing advances in EUVL technology as the driving force in the development of picometer-level equipment, aiming at feature sizes of 10 nm and beyond.

The first international conference with 'EUVL' in the title was held near Mt. Fuji in 1993. In his opening address, Dr. Kinoshita said, 'As long as we do not lose the desire that has sprung from within us, technology will steadily advance from the micro to the nano to the pico'.

References

[1] H. Kinoshita, R. Kaneko, K. Takei, N. Takeuchi and S. Ishihara, JSAP, 28-ZF-15 (1986) [in Japanese].
[2] H. Kinoshita, K. Kithara, Y. Ishii and Y. Torii, J. Vac. Sci. Technol. B 7, 1648 (1989).
[3] H. Takenaka, Y. Ishiii, H. Kinoshita and K. Kurihara, Proc. SPIE. 1345, 213 (1990).
[4] H. Kinoshita, K. Kurihara and H. Takenaka, Jpn. J. Appl. Phys. 30, 3048 (1991).
[5] K. Kurihara, H. Kinoshita, T. Mizota, T. Haga and Y. Torii, J. Vac. Sci. Technol. B 9, 3189 (1991).
[6] H. Kinoshita, K. Kurihara, T. Mizota, T. Haga, H. Takenaka, et al., Appl. Opt. 32, 7079–7083 (1993).
[7] T. Haga and H. Kinoshita, J. Vac. Sci. Technol. B 13, 2914 (1995).
[8] T. Haga, M. C. K. Tinone, H. Takenaka and H. Kinoshita, Microelectron. Eng. 30, 179–182 (1996).
[9] H. Kinoshit and T. Watanabe, J. Photopolym. Sci. Technol. 13, 379–384 (2000).
[10] H. Kinoshita and T. Watanabe, Jpn. J. Appl. Phys. 39, 6771 (2000).
[11] H. Kinoshita, T. Watanabe, Y. Li, A. Miyafuji, T. Oshino, et al., Proc. SPIE. 3997, 70 (2000).
[12] K. Hamamoto, T. Watanabe, H. Tsubakino, H. Kinoshita, T. Shoki, et al., J. Photopolym. Sci. Technol. 14, 567 (2001).
[13] K. Hamamoto, T. Watanabe, H. Hada, H. Komano, S. Kishimura, et al., Proc. SPIE. 4688, 664 (2002).
[14] Y. Fukushima, T. Watanabe, R. Ohnishi, H. Kinoshita, H. Shiotani, et al., J. Photopolym. Sci. Technol. 20, 419–422 (2007).
[15] T. Watanabe, Y. Fukushima, H. Shiotani, R. Ohnishi, S. Suzuki, et al., Jpn. J. Appl. Phys. 46, 6118 (2007).
[16] Y. Fukushima, T. Watanabe, R. Ohnishi, H. Shiotani, S. Suzuki, et al., Jpn. J. Appl. Phys. 46, 6198 (2007).
[17] Y. Yamaguchi, Y. Fukushima, T. Iguchi, H. Kinoshita, T. Harada, et al., J. Photopolym. Sci. Technol. 23, 681–686 (2010).
[18] Y. Fukushima, N. Sakagami, T. Kimura, Y. Kamaji, T. Iguchi, et al., Jpn. J. Appl. Phys. 49, 06GD06 (2010).
[19] Y. Fukushima, Y. Yamaguchi, T. Kimura, T. Iguchi, T. Harada, et al., J. Photopolym. Sci. Technol. 23, 673–680 (2010).

[20] T. Urayama, T. Watanabe, Y. Yamaguchi, N. Matsuda, Y. Fukushima, et al., J. Photopolym. Sci. Technol. 24, 153–157 (2011).
[21] H. Kinoshita, T. Haga, K. Hamamoto, S. Takada, N. Kazui, et al., J.Vac.Sci.Technol. B22, 264–267 (2004).
[22] K. Hamamoto, Y. Tanaka, T. Yoshizumi, N. Hosokawa, N. Sakaya, et al., Jpn. J. Appl. Phys. 45, 5378 (2006).
[23] H. Kinoshita, K. Hamamoto, N. Sakaya, M. Hosoya and T. Watanabe, Jpn. J. Appl. Phys. 46, 6113 (2007).
[24] T. Harada, J. Kishimoto, T. Watanabe, H. Kinoshita and D. G. Lee, J. Vac. Sci. Technol. B 27, 3203 (2009).
[25] T. Harada, M. Nakasuji, T. Kimura, T. Watanabe, H. Kinoshita, et al., J. Vac. Sci. Technol. B 29, 06F503 (2011).
[26] T. Harada, M. Nakasuji, M. Tada, Y. Nagata, T. Watanabe, et al., Jpn. J. Appl. Phys. 50, 06GB03 (2011).
[27] T. Harada, M. Nakasuji, T. Kimura, Y. Nagata, T. Watanabe, et al., Proc. SPIE. 8081, 80810K (2011).
[28] H. Kinoshita, T. Harada, M. Nakasuji, Y. Nagata and T. Watanabe, Microelectron. Eng. 88, 2000–2003 (2011).
[29] M. Nakasuji, A. Tokimasa, T. Harada, Y. Nagata, T. Watanabe, et al., Jpn. J. Appl. Phys. 51, 06FB09 (2012).
[30] T. Harada, Y. Tanaka, T. Amano, Y. Usui, T. Watanabe, et al., Proc SPIE. 9048, 90483F (2014).
[31] Y. Platonov, J. Rodriguez, M. Kriese, E. Gullikson, T. Harada, et al., Proc. SPIE. 8076, 80760N (2011).